Chin. Geogra. Sci. 2022 Vol. 32 No. 5 pp. 834−851
https://doi.org/10.1007/s11769-022-1304-2

Springer Science Press
www.springerlink.com/content/1002-0063

An Investigation of Landslide Susceptibility Using Logistic Regression and Statistical Index Methods in Dailekh District, Nepal

Dil Kumar RAI[1,2], XIONG Donghong[1,3], ZHAO Wei[1,3], ZHAO Dongmei[1,2], ZHANG Baojun[1], Nirmal Mani DAHAL[1,2], WU Yanhong[1,3], Muhammad Aslam BAIG[1,2]

(1. *Institute of Mountain Hazards and Environment* (*IMHE*), *Chinese Academy of Sciences*, *Chengdu* 610041, *China*; 2. *University of Chinese Academy of Sciences*, *Beijing* 100049, *China*; 3. *Kathmandu Center for Research and Education*, *Chinese Academy of Sciences-Tribhuvan University*, *Kathmandu* 44613, *Nepal*)

Abstract: Landslide distribution and susceptibility mapping are the fundamental steps for landslide-related hazard and disaster risk management activities, especially in the Himalaya region which has resulted in a great deal of death and damage to property. To better understand the landslide condition in the Nepal Himalaya, we carried out an investigation on the landslide distribution and susceptibility using the landslide inventory data and 12 different contributing factors in the Dailekh district, Western Nepal. Based on the evaluation of the frequency distribution of the landslide, the relationship between the landslide and the various contributing factors was determined. Then, the landslide susceptibility was calculated using logistic regression and statistical index methods along with different topographic (slope, aspect, relative relief, plan curvature, altitude, topographic wetness index) and non-topographic factors (distance from river, normalized difference vegetation index (NDVI), distance from road, precipitation, land use and land cover, and geology), and 470 (70%) of total 658 landslides. The receiver operating characteristic (ROC) curve analysis using 198 (30%) of total landslides showed that the prediction curve rates (area under the curve, AUC) values for two methods (logistic regression and statistical index) were 0.826, and 0.823 with success rates of 0.793, and 0.811, respectively. The values of *R*-Index for the logistic regression and statistical index methods were 83.66 and 88.54, respectively, consisting of high susceptible hazard classes. In general, this research concluded that the cohesive and coherent natural interplay of topographic and non-topographic factors strongly affects landslide occurrence, distribution, and susceptibility condition in the Nepal Himalaya region. Furthermore, the reliability of these two methods is verified for landslide susceptibility mapping in Nepal's central mountain region.

Keywords: landslide characteristics; landslide susceptibility; logistic regression; statistical index; Nepal Himalaya

Citation: Dil Kumar RAI, XIONG Donghong, ZHAO Wei, ZHAO Dongmei, ZHANG Baojun, Nirmal Mani DAHAL, WU Yanhong, Muhammad Aslam BAIG, 2022. An Investigation of Landslide Susceptibility Using Logistic Regression and Statistical Index Methods in Dailekh District, Nepal. *Chinese Geographical Science*, 32(5): 834−851. https://doi.org/10.1007/s11769-022-1304-2

1 Introduction

The Himalayan Mountain range is the most prone area to landslide, with about 75% of global landslides occurring in Southwestern China, Nepal, India, Laos, Myanmar, Bangladesh, Philippines, and Indonesia (Froude and Petley, 2018). Due to seasonal variations in precipitation affected by the EI Nino-Southern Oscillation (ENSO) (Emberson et al., 2021), more and more landslides occurred in this region, combined with frequent

Received date: 2021-07-27; accepted date: 2021-11-07
Foundation item: Under the auspices of the CAS Overseas Institutions Platform Project (No. 131C11KYSB20200033), the National Natural Science Foundation of China (No. 42071349), the Sichuan Science and Technology Program (No. 2020JDJQ0003)
Corresponding author: ZHAO Wei. zhaow@imde.ac.cn

catastrophic floods (Kale, 2012; Wei et al., 2020). The weakened relationship between ENSO and Indian summer monsoon rainfall (ISMR) has been restored in the last decades of 2000−2018 compared to earlier decades of 1979−1997 (Yang and Huang, 2021), and it is reflected by the mutual interaction of landslides, ENSO-induced intensity of rainfall, and cascading catastrophic flooding in southern Asia. Besides the external factors caused by the climate change, the steep topography, the great variations in topographic relief, the active tectonic movement with persistent fault motion, the tectonic uplift, and the fractured lithology are also the main influencing factors for the landslide in the Himalaya Mountain and its adjacent regions (Mandal and Mandal, 2018; Xue et al., 2021).

As an important part of the Himalaya Mountain regions, Nepal Himalaya contributes 10% of all landslides induced by monsoon rainfall in the global dataset (Froude and Petley, 2018). The geomorphologic, and geological conditions, bedrock hydrology, clay minerals, soil characteristics, earthen road construction, land use and land cover change, and prolonged intense precipitation have been defined as the most proxy intrinsic and extrinsic contributing factors for landslide activities (Hasegawa et al., 2009; Ghimire, 2011, 2017; Regmi et al., 2013b; Dahal, 2009, 2014; Adhikari et al., 2022). Therefore, these contributing factors have been identified by previous landslide susceptibility analyses (Ghimire, 2011; Devkota et al., 2013; Regmi et al., 2014c; Meena et al., 2019; Dhakal et al., 2020b). For instance, the rock toppling falls are more proactive in the Maure Khola landslides caused by Nourpoul geological formations consisting of amphibolite, quartzite, slate/phyllite at Mugling-Narayanghat road section (Regmi et al., 2014b). A reduction of rock strength due to the clay minerals, rainfall, wide fault zone, and extreme weather predominately initiated the large Dumrebesi landslide in the Lesser Himalaya, Nepal (Regmi et al., 2013a). Different geological attributes such as weathered rocks, joint infillings, and shear zones with rich clay minerals, including hydrologic, climatic, and anthropogenic factors accelerated the development of the large Taprang landslide in west Nepal (Regmi et al., 2017). Extensive hydrothermal alteration during the advancement of Main Central Thrust (MCT), clay minerals in the sliding zones of large-scale landslides, slope failure during the monsoon rainfall are the major causes of large-scale landslides in the Lesser Himalaya of Nepal (Hasegawa et al., 2009). The Gorkha earthquake with Mw 7.8 in 2015 and aftershock characteristics, slope distributions, the effect of precipitation on rock strength via weathering, and change in vegetation cover mutually triggered about 25 000 landslides in Nepal (Roback et al., 2018).

To better understand the landslide characteristics in Nepal Himalaya, many studies have been conducted regarding landslide characteristics covering different regions (Zhang et al., 2016; Guo et al., 2017; Martha et al., 2017; Tiwari et al., 2017; Roback et al., 2018; Thapa, 2018; Dhakal et al., 2020a). These studies are crucial for the evaluation for landslide hazards and implementation of disaster reduction strategies (Kubwimana et al., 2021). Additionally, landslide susceptibility, referring to the likelihood of landslide occurrence in a given area based on local terrain and environmental conditions (Guzzetti et al., 1999), has attracted much attention in recent years. Different statistical methods have been evaluated to generate the landslide susceptibility maps, such as the weight of evidence (Dahal et al., 2008), artificial neural networks and frequency ratio (Poudyal et al., 2010), and bivariate statistical index (Ghimire, 2011; Pradhan et al., 2012; Bijukchhen et al., 2013). Similarly, logistic regression (Devkota et al., 2013; Zhang et al., 2019), heuristic and bivariate statistical index (Bijukchhen et al., 2013), frequency ratio and conditional probability (Regmi et al., 2014c), hybrid spatial multicriteria evaluation (HSMCE) (Meena et al., 2019), and certainty factor (Dhakal et al., 2020b) have been evaluated. Among these methods, quantitative multivariate logistic regression and bivariate statistical index methods exhibited good performance in predicting landslide susceptibility in the context of Nepal Himalaya (Ghimire, 2011; Pradhan et al., 2012; Bijukchhen et al., 2013; Devkota et al., 2013; Linkha et al., 2019; Ghimire and Timalsina, 2020).

In this respect, aiming to better understand the landslide condition in the Nepal Himalaya, the Dailekh District in the Western Nepal, which has experienced many types of landslides for several years causing remarkable loss of lives and damages to physical infrastructures, was selected as the study area due to its unclear landslide characteristics including distribution and its susceptibility condition. Based on the logistic regression and statistical index methods, the major objectives of

this study are as follows: 1) analyzing distribution of landslide frequency in relation to 12 different topographic and non-topographic factors, and 2) landslide susceptibility mapping using the logistic regression and bivariate statistical index methods. This research is a representative and specific study of the middle mountain areas of the Nepal Himalaya and provides important knowledge information about the landslide distribution and susceptibility conditions.

2 Study Area and Data

2.1 Study area

Administratively, the Dailekh District is located in the Karnali Province of Nepal. The district covers an area of 1482.98 km^2, and positioned at 81°24′36″E to 81°55′36″E and 28°38′00″N to 29°08′10″N (Fig. 1). The altitude of the district ranges from 554 m (Tallo Dungeshower) to 4017 m (Mahabu Lek). The general geographical features of the district are southward-facing slopes associated with two distinct physiographic regions, namely, the middle hills or lesser Himalaya, and the high mountain region (Dhital, 2015).

The physiographic characteristics of the high mountain region are a southward-facing slope and rugged topographic features, where there is no anthropogenic activity, acting as the sources of water towers for the lowland areas, and the surface is covered with diverse vegetation species of the temperate evergreen forest and open grassland. The middle hill region of the Dailekh District is characterized by different topographical aspects associated with gentle steep hillslopes, dense presences of streams accumulated into the nearby mainstream flow. A wide range of alluvial-deposited flood plains along the rivers originated at the first-order catchment of the south-facing upland of the high mountain regions such as Chhamgad, Lohore, Ramgad, Parajul, and Paduka, including the transboundary Karnali River of China, India, and Nepal. The cultural landscape exhibits dense population, terracing the slopes for cultivation and vertical upward and downward movement of local inhabitants for the upland (hillslope) and lowland (alluvial-deposited flat land) based cultivation activities. The major vegetation species are tropical and subtropical forest types as present along the steep side of the rivers, whereas the upland areas have evergreen temperate forest coverage including alpine species. The climate condition and its variability of the study area depend on the physiographic characteristics and monsoon rainfall, which are tropical, temperate, and subalpine. The major land-use and land-cover features are agriculture, forest, shrub, and grassland. This region is characterized by four types of climate zones based on the altitude, namely, tropical (below 1000 m), subtropical (1000−2000 m), temperate (2000−3000 m), and subalpine climate zone (3000−4000 m).

2.2 Landslide inventory data

Determination of actual landslide information, including the location, size, and spatial distribution, is a prerequisite and fundamental step in landslide studies (Guzzetti et al., 2005). In this study, the landslide data of the study area were generated via direct visual image interpretation of Google Earth based satellite images

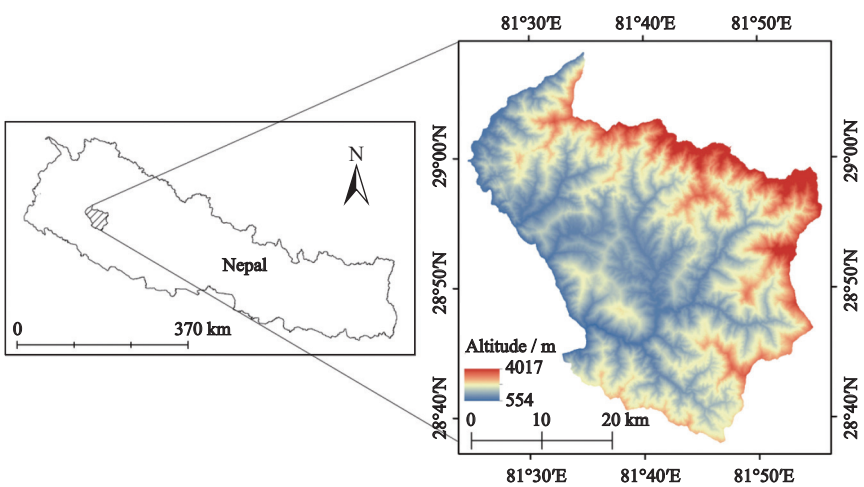

Fig. 1 Location of Dailekh District in Nepal and its altitude

and topographical maps obtained from the Department of Survey, Nepal Government. The Google Earth interface is one of the most dependable sources for generating actual landslide data from satellite images via direct visual image interpretation (Schmid et al., 2015; Linkha et al., 2019). Then, the observed landslide data were categorized and standardized based on the classification of Varnes (1978) including landslide forms, size, material content, and mechanism.

2.3 Landslide triggering factors

Generally, the major landslide triggering factors can be categorized into topographic and non-topographic groups (Robinson et al., 2017). In this study, the topographic factors include slope, aspect, curvature, relative relief, altitude, topographic wetness index (TWI), whereas the non-topographic factors are distance from road, distance from river, precipitation, geology, normalized difference vegetation index (NDVI), and land use and land cover (LULC).

2.3.1 Topographic factors

In general, the topographical factors were obtained from the topographical maps on a scale of 1 : 25 000 developed by the Department of Survey, Nepal Government. The slope was considered following the principle that an increase in the degree of slope increases the likelihood of a landslide (Mandal and Mandal, 2018). It was calculated using the contour-derived DEM data with 20 m spatial resolution. The slope gradient is categorized into five categories (Fig. 2a). The slope aspect indicates slope facing towards different directions associated with different characteristics such as receiving precipitation pattern, moisture and humidity retention, and the presence of vegetation; these attributes influenced the occurrence of landslides. The aspect can be grouped into nine distinct groups: 1) Flat; 2) North

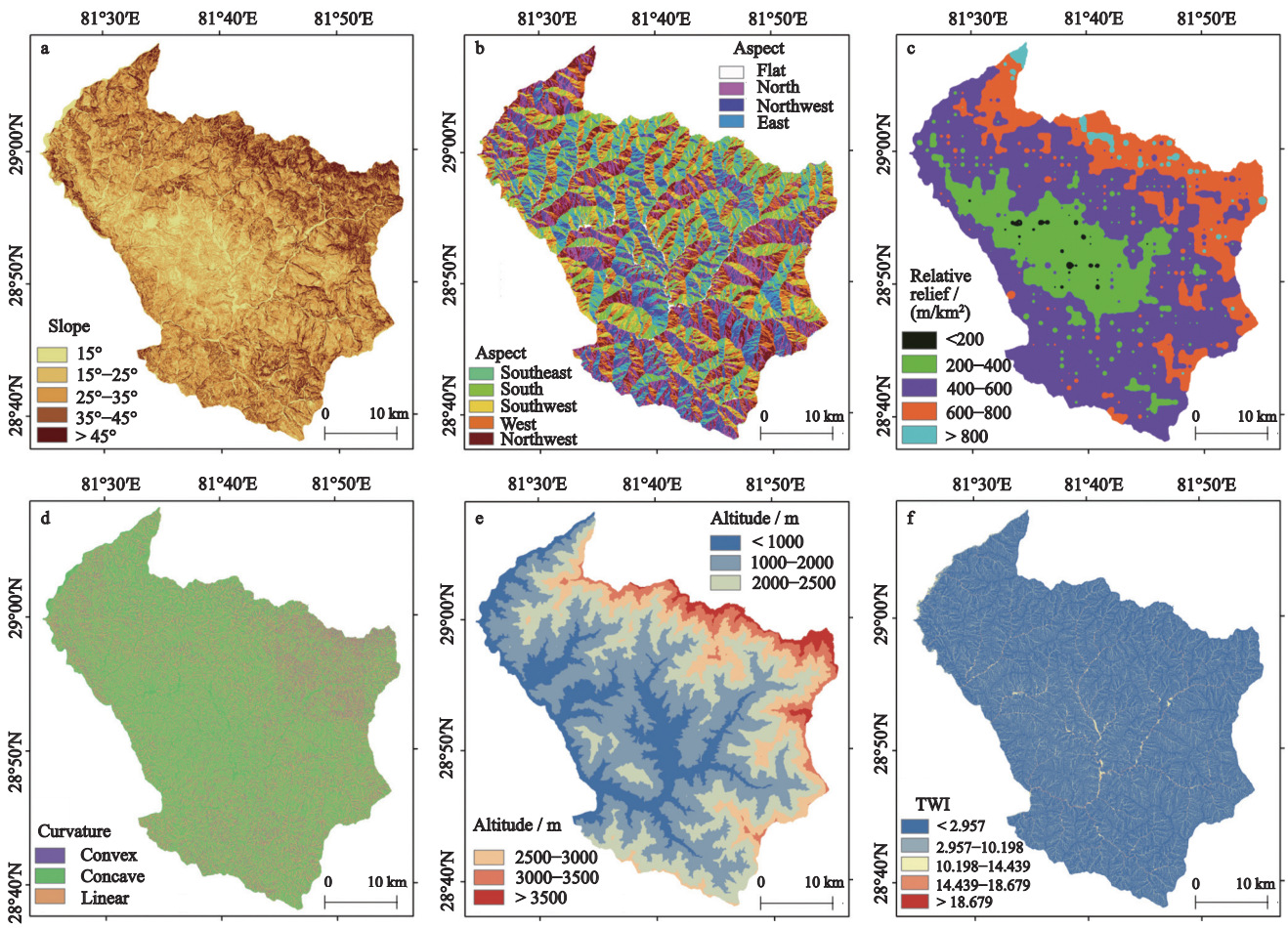

Fig. 2 Thematic of the topographic factors of the Dailekh district in the Western Nepal. a. slope; b. aspect; c. relative relief; d. plan curvature; e. altitude; f. topographic wetness index (TWI)

(337.5°−22.5°); 3) Northeast (22.5°−67.5°); 4) East (67.5°−112.5°); 5) Southeast (112.5°−157.5°; 6) South 157.5°−202.5°); 7) Southwest (202.5°−247.5°); 8) West (247.5°−292.5°); 9) Northwest (292.5°−337.5°) (Fig. 2b). The relative relief represents local variations in elevation within a certain area. It is assumed that an increase in the local height facilitates the formation of sufficient energy for the landslide. It was also calculated using the contour-derived DEM data and divided into five categories (Fig. 2c).

The curvature represents surface's curve shape. High convexity and concavity usually will lead to flow accumulation on the surface, resulting in slope saturation and instabilities. It was categorized into three types such as convex, concave, and flat curve shape (Fig. 2d). Moreover, altitude is also an important factor for landslide, was divided into six categories (Fig. 2e). Then, the TWI concept provided by Beven and Kirkby (1979), which refers to the location and size of saturated areas subjected to overflow, runoff generation, and long-term moisture availability in the landscape (Wilson and Gallant, 2000; Kopecký and Čížková, 2010). Commonly, TWI is used to quantify the topographic control on hydrological processes (Devkota et al., 2013).

$$TWI = \mathrm{Ln}\frac{\alpha}{\tan\beta} \tag{1}$$

where, α represents the cumulative upslope area draining through a point (per unit contour length) and $\tan\beta$ is slope angle at the point. The TWI factor was classified into five classes according to the natural break method (Fig. 2f).

2.3.2 Non-topographic factors

The distance from river generated as the controlling factor in terms of stream saturation determines the slope stability and erodes of the toe slopes (Bijukchhen et al., 2013). It was calculated from the river data of topographic data and classified into different types (Fig. 3a). A close distance from river indicates a high possibility of hillslope processes that result in slope instabilities such as landslide and slope failures. Similarly, the NDVI measures the density of surface vegetation cover, which influences the foundation of landslides on steep slopes. The NDVI index was calculated from the surface reflectance of near-infrared (*NIR*) band and red (*R*) band of the Landsat 8 OLI/TIRS observations:

$$\mathrm{NDVI} = \frac{NIR - R}{NIR + R} \tag{2}$$

The NDVI value ranges between 0 to 1 and can be classified into five types (Fig. 3b).

Roads are one of the major human-induced contributing factors of landslides in Nepal, leading to substantial land degradation (Linkha et al., 2020). Therefore, current road data were generated by visually interpreting the Google Earth images, by considering all road types, including earthen, graveled, and blacktopped roads. Distance from the road can be divided into seven types (Fig. 3c).

The precipitation pattern and intensity directly affect the occurrence of landslides in mountainous areas. Hence, the satellite-based WorldClim data (https://worldclim.org/data/monthlywth.html) from 1999 to 2018 were used as a precipitation factor for this analysis. The maximum annual precipitation from 1999 to 2018 were used to evaluate the landslide distribution pattern and susceptibility. It was assumed that the maximum intensity of precipitation produced adequate energy to cause the landslides on the steep hillslope. Therefore, this factor was categorized into different types (Fig. 3d). The LULC data was produced using a supervised classification method with Landsat 8 observations and there are seven types (Fig. 3e): agricultural land (76.4%), forest (18.8%), grassland (2.27%), shrubland (2.27%), barren land (0.15%), and river or water body (0). The spatial extent of the LULC features was taken as the key triggering factors for landslide because the condition of LULC plays a crucial role in causing the environmental hazards in Nepal (Paudel et al., 2016; Chidi et al., 2021).

Geology also plays a significant role on the occurrence of landslides because lithological and structural differences frequently result in differences in soil and rock strength and permeability (Gerrard, 1994; Shroder and Bishop, 1998; Hasegawa et al., 2009; Regmi et al., 2013a). According to the geological map (1 : 250 000) of study area developed by the Department of Mines and Geology, Nepal Government, different lithological formations are found in the Dailekh District such as: 1) the Ulleri formation (UF); 2) the Salyanigad formation (SF); 3) the Ranimatta formation (RF); 4) the Palezoic granite (PG); 5) the Kusma formation (KuF); 6) Kalikot formations GH (KF(GH)); 7) Kalikot formation Bu

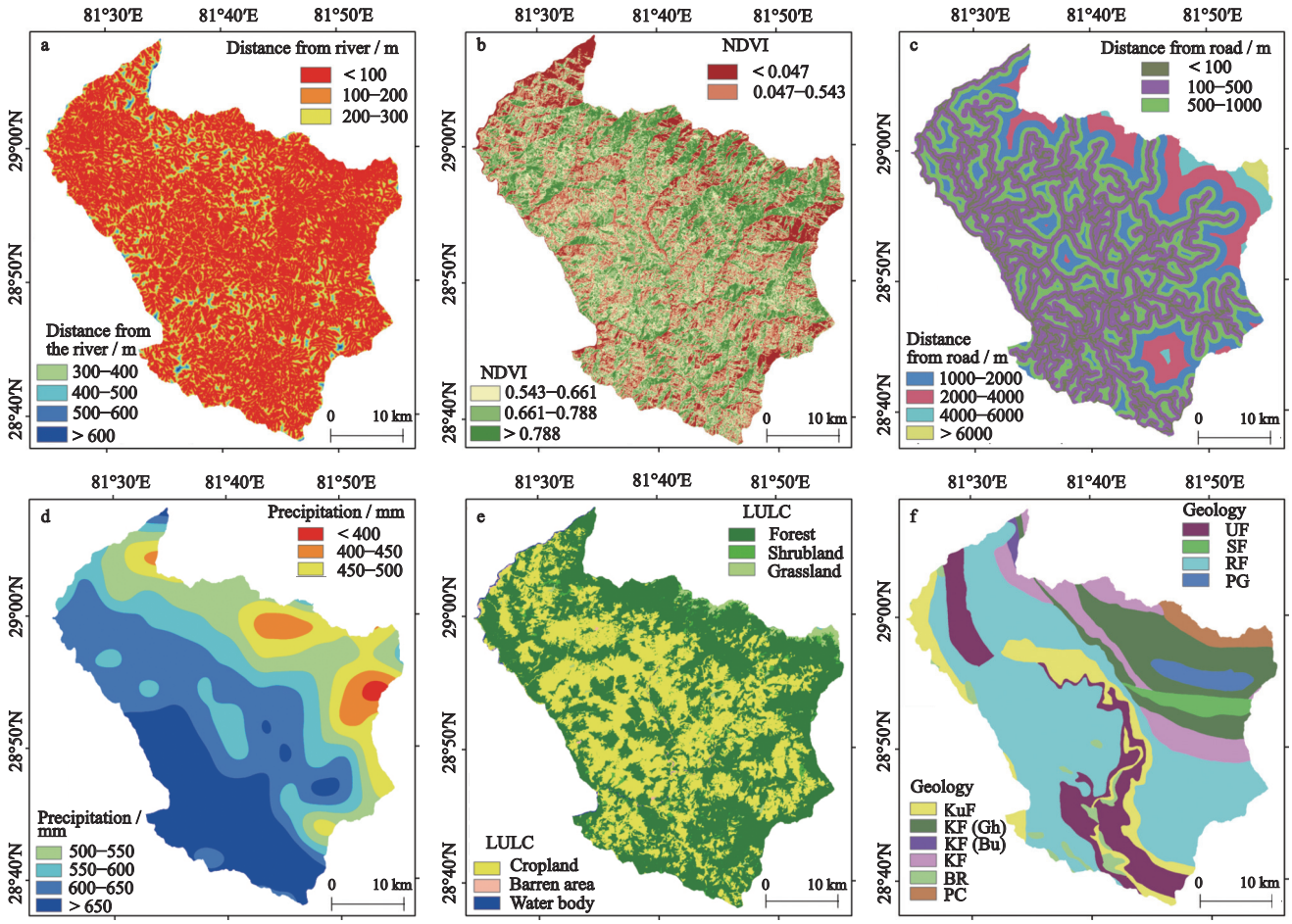

Fig. 3 Thematic maps of non-topographic factors of the Dailekh district in the Western Nepal: a. distance from river, b. normalized difference vegetation index (NDVI); c. distance from road, d. precipitation, e. land use and land cover (LULC), and f. geology. UF, the Ulleri formation; SF, the Salyanigad formation; RF, the Ranimatta formation; PG, the Palezoic granite; KuF, the Kusma formation; KF(GH), Kalikot formations GH; KF(Bu), Kalikot formation Bu; KF, Kalikot formation; BR, Basic rock; PC, Proterozoic Crystallines

(KF(Bu)); 8) Kalikot formation (KF); 9) Basic rock (BR); 10) Proterozoic Crystallines (PC) (Fig. 3f).

3 Susceptibility Assessment Method

3.1 Susceptibility assessment method

3.1.1 Multivariate logistic regression

Multivariate logistic regression has been widely used for landslide susceptibility concerning triggering factors (Lin et al., 2017; Reichenbach et al., 2018). This method is useful when the result-dependent variables are binary or dichotomous. The presence or absence of a landslide is the dependent variable in this analysis (Bhandary et al., 2013). In logistic regression analysis, the independent variables, such as x_1, x_2, x_3, … x_n, triggering landslide occurrences are defined, where the logit model y is assumed as a linear combination of independent variables, which can be expressed as follows:

$$y = b_0 + b_1x_1 + b_2x_2 + b_3x_3 + \cdots + b_nx_n \quad (3)$$

where y is the dependent variable represented by binary variables such as 0 or 1 showing the landslide absence or presence, respectively; x_1, x_2, x_3,… x_n are the explanatory variables; b_0 is a constant of the equation; b_1, b_2, b_3, … b_n are regression coefficients for the explanatory variables. The relationship between landslide occurrences and its dependency on explanatory variables can be written as:

$$P = 1/1 + e^{-y} \quad (4)$$

where P represents the estimated conditional probability of landslide occurrences. Eqs. (3) and (4) show that the natural logarithm of the odds, Ln(P/1−P) is linearly related to independent variables (Dahal, 2014):

$$\mathrm{Ln}\left(P/1-P\right)=b_0+b_1x_1+b_2x_2+b_3x_3+\cdots+b_nx_n \quad (5)$$

For the landslide susceptibility mapping, various topographic and non-topographic based factors were used as the explanatory variables. The independent variables in the form of the geospatial shape layers, as well as their corresponding coefficients and constants were fitted into the logistic regression equation to generate the landslide susceptibility map under the GIS interface environment, which can be written as:

$$\mathrm{Logit}(y)=constant+\beta_1V_1+\beta_2V_2+\beta_3V_3+\beta_4V_4+\beta_5V_5+\beta_6V_6+\beta_7V_7+\beta_8V_8+\beta_9V_9+\beta_{10}V_{10}+\beta_{11}V_{11}+\beta_{12}V_{12} \quad (6)$$

where β_i (i = 1, 2, 3, …12) represents the coefficient of each variable in the model, and V_1 to V_{12} correspond to the six topographic variables (slope, aspect, curvature, relative relief, altitude; TWI) and the six non-topographic variables (distance from road, distance from river, precipitation, geology, NDVI, and LULC).

3.1.2 Bivariate statistical index

The bivariate statistical index model, developed by Van Western (1997) has been commonly applied to generate the landslide susceptibility. In this method, a weight value of each parameter class is defined as the natural logarithm of the landslide density in class divided by the landslide density in the whole map:

$$w_i=\mathrm{In}\left(\frac{denseClass}{denseMap}\right)=\mathrm{In}\left(\left(\frac{N_{pix}(s_i)}{N_{pix}(N_i)}\right)\Big/\left(\frac{\sum N_{pix}(s_i)}{\sum N_{pix}(N_i)}\right)\right) \quad (7)$$

where w_i is the weight assigned to the parameter class i, *densClass* is the landslide density within the parameter class, and *denseMap* represents the landslide density for the entire study area. *Npix* (S_i) is the total number of pixels that comprise landslide in a parameter class i, and N_{pix} (N_i) represents the total pixels in the same parameter class. Then, the final landslide susceptibility index was calculated using calculated weight values of all thematic parameters, which can be expressed as:

$$LSI=\sum_{j=1}^{n}W_{ij} \quad (8)$$

where, *LSI* is the landslide susceptibility index, n is the number of parameters and W_{ij} is the sum weight of any class i of j parameter. The bivariate statistical index method is based on the statistical correlation of the landslide inventory map with illustrative attributes of parameter maps. i.e., w_i is only calculated for landslide-occurred classes (Kavzoglu et al., 2015). In the context of the Nepal Himalaya, some earlier studies successfully applied and proved the relevance of statistical-based index methods to evaluate landslide susceptibility (Ghimire, 2011; Bijukchhen et al., 2013).

3.2 Evaluation method

3.2.1 Receiver operating characteristic (ROC) curve

A ROC curve analysis was conducted to validate the accuracy of the susceptibility assessment with the AUC in this study, which has been widely used to validate the degree of prediction of landslide susceptibility mapping. The ROC curve was prepared with a combination of sensitivity: false positive rate and true positive rate, where the x-axis represents specificity and the y-axis represents sensitivity that represents the degree of accuracy of regression between landslide occurrences and non-occurrences. The ROC curve was successfully applied to previous landslide susceptibility mapping works in Nepal (Devkota et al., 2013). The formula for calculation of specificity and sensitivity can be written as:

$$X=1-\left[\frac{TN}{TN+FP}\right] \quad (9)$$

$$Y=\left[\frac{TP}{TP+FN}\right] \quad (10)$$

where X is the true positive rate (1-specificity), Y is the false positive rate (sensitivity), *TN* is true negative, *FP* is false positive, *TP* is true positive, and *FN* is false negative.

3.2.2 Relative landslide density (*R*-Index)

The relative landslide density (*R*-Index) was applied to evaluate the accuracy of landslide susceptibility prediction, which is commonly used for landslide susceptibility result validation (Bijukchhen et al., 2013; Meena et al., 2019; Wubalem and Meten, 2020) and can be expressed as:

$$R\text{-Index}=\frac{\frac{n_i}{N_i}}{\sum\frac{n_i}{N_i}\times 100} \quad (11)$$

where n_i denotes the number of observed landslides within a susceptibility index class and N_i is the area of the cells of this class.

4 Results

4.1 Landslide inventory and mapping

A detailed description of the observed landslides was analyzed based on the distribution pattern, type, and area in this study. A total of 658 landslides occurred in 1988–2020 were identified (Fig. 4), including both old and new patches, with a total coverage area of approximately 908.18 ha. The average area is 1.37 ha; the largest area is 23.92 ha; and the smallest area is 0.02 ha. The standard deviation of all the landslide area is 2.34 ha. Shallow, translational, and rotational deep-seated landslides were observed in the study area. The shallow landslides are associated with a cohesive combination of colluvium rock, soil materials, rich permeability soil, leading to slope failure of water infiltration into the bottom (Selby, 1982). The deep-seated landslides occurred with the materials such as deep regolith, colluvium materials, and weathered rock (Chorley et al., 1985). The diverse topographic and non-topographic factors influenced the spatial distribution of landslides, which further demonstrated a dispersed or scattered distribution pattern in the study area.

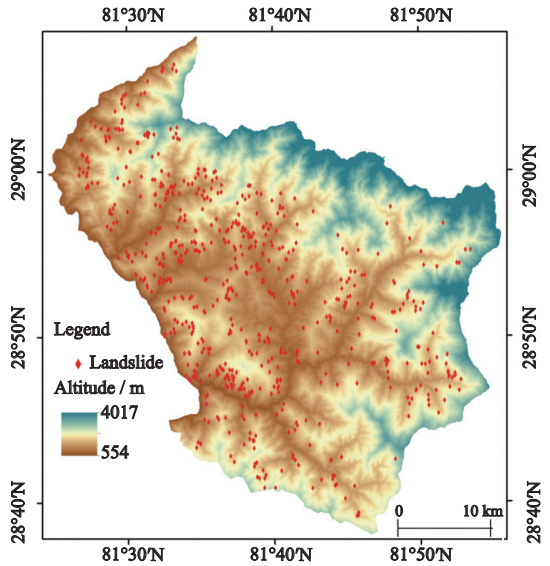

Fig. 4 Distribution of the detected landslides of the Dailekh District in the Western Nepal from 1988 to 2020

4.2 Spatial distribution of landslides

4.2.1 Topographic distribution

Slope gradients are strongly associated with landslide distribution, in terms of higher landslide occurrences with increased slope gradients (Mandal and Mandal, 2018). Most of the observed landslides approximately 92.2% of total landslides occurred at slopes between 15° and 45° in the study area. Fewer landslides (about 7.5% of total landslides) occurred at slopes below 15°, and only 0.3% of total landslides occurred on the high steep slopes above 45° (Fig. 5a). It revealed that the mechanisms involved in the formation of the landslides are significantly activated on the moderately steep slopes. The high steep slopes demonstrated less remarkable processes to landslide occurrences and slope instability. The directional aspects of the slopes have a strong relationship with the landslide incidents and their morphometric characteristics. The analysis showed that 93.7% of the landslides were dispersed in the different aspects such as the east, south, and west slope of the topography, whereas only 6.3% of the landslides were distributed in the north side of the topography (Fig. 5b).

Similarly, the relative relief shows a good relationship with landslide occurrences: the high presence of landslide distribution was associated with an increase in the relative relief threshold (m/km^2). The distribution pattern revealed that approximately 89.6% of the total landslides occurred in the local relative relief ranges between 300 and 600 m/km^2, and the remaining landslides were distributed in the low relative relief of less than 300 m/km^2. The increased relative relief causes slope instabilities, which promote avenue conditions for landslide occurrence in mountainous areas (Fig. 5c). Moreover, the analysis also showed that most of the observed landslides are distributed on the convex and concave curvatures of the ground surfaces (Fig. 5d). Among the total observed landslides, about of 94.3% of landslides are associated with convex and concave curvatures, and a smaller number of landslides of about 5.7% of landslides existed on the linear curvature. Regarding the elevation distribution, the majority of the observed landslides occurred between 500 m and 2500 m. Among them, 23% of landslides existed in elevations below 1000 m, and 61.5% of landslides were distributed in elevations between 1000−1500 m. An elevation between 1500–2500 m occupies 15.5% of the total landslides (Fig. 5e). No landslides were observed in the elevations above 2500 m in the study area. The TWI belongs to heterogeneous topography indicating the landslide occurrences. The very high (>12.110) saturated

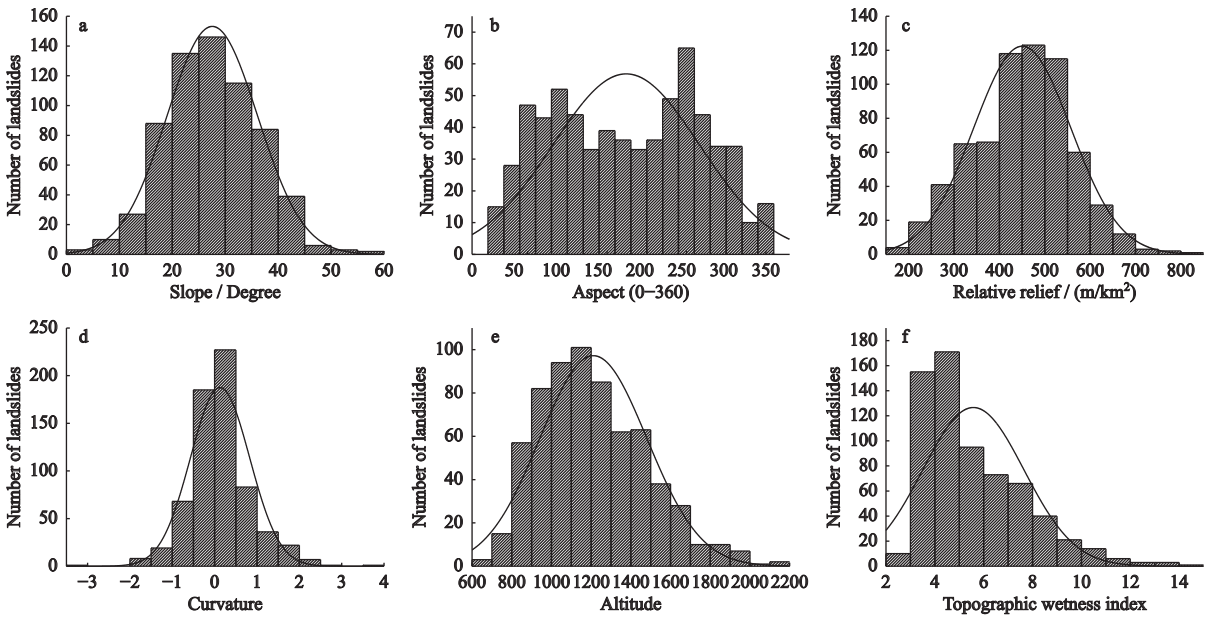

Fig. 5 Distribution of landslides of the Dailekh District in the Western Nepal with different topographic factors. a. slope gradient; b. aspect; c. relative relief; d. curvature; e. altitude; f. topographic wetness index (TWI)

areas represent such 'areas' mainstream flow line on the flat surface. Hence, a number of landslides were observed. In contrast, more than two-thirds (98%) observed landslides occurred in the low to very high (< 4.460 and > 12.110) wetness index areas (Fig. 5f).

4.2.2 Non-topographic distribution

The non-topographical factors also show a coherent relationship with landslide distribution characteristics in the study area. As shown in Fig. 6a, the major landslides occurred within a close distance from rivers in the study area. More than 98% of the observed landslides were found within 300 m close distance of rivers. It revealed that the hydrogeophysical function of the channel stream has a good connection to the evolution of slope dissection and failure, which resulted in a substantial occurrence of landslides. Moreover, the positive and negative roles of NDVI were observed in terms of the distribution of the observed landslides. Most of the observed landslides are mainly distributed in areas with low-to-moderate NDVI values (Fig. 6b). In this condition, the vegetation, bush and grassland are low density, and the frequency of landslide is very high. Comparatively, the high NDVI values, representing good vegetation cover, prevented landslide occurrence and there were few landslides in this region. The proximity to the road is strongly correlated to the distribution of landslide. Approximately 70% of all landslides were distributed within the 100 m distance from road (Fig. 6c). This result indicated that road construction by dissecting a stable slope terrain helps to increase the likelihood of landslides in Nepal (Petley et al., 2007). A condition revealed that the occurrence of land degradation is associated with the opening of earthen roads in steep hillslopes (Linkha et al., 2020).

Regarding the relationship with precipitation, significant influences of precipitation on landslide occurrence have been recognized by many previous studies (Dhital et al., 1993; Dahal and Hasegawa, 2008; Manchado et al., 2021). This impact was also apparently revealed in this study: approximately 95% of all landslides occurred at the high precipitation regime of above 550 mm, and only a fewer landslides occurred at the low regime of precipitation (Fig. 6d). The middle hill region received a high intensity of precipitation, which triggered substantial occurrences of landslides. In contrast, limited number of landslides occurred in high mountain regions due to low precipitation. In the study area, the topographic attributes and local wind directions influenced the spatial pattern and intensity of precipitation (Zhang et al., 2016). The observed landslides occurred in various types of geological formations (Fig. 6e). About 88.7% of the observed landslides occurred in the Ranimatta, Ulleri, and Kushma formations, representing 66.7%, 11.55%, and 10.48% of this total, respectively. Other formations such as the Kalikot formation, Palezoic granite, basic rock, and salyani Gad

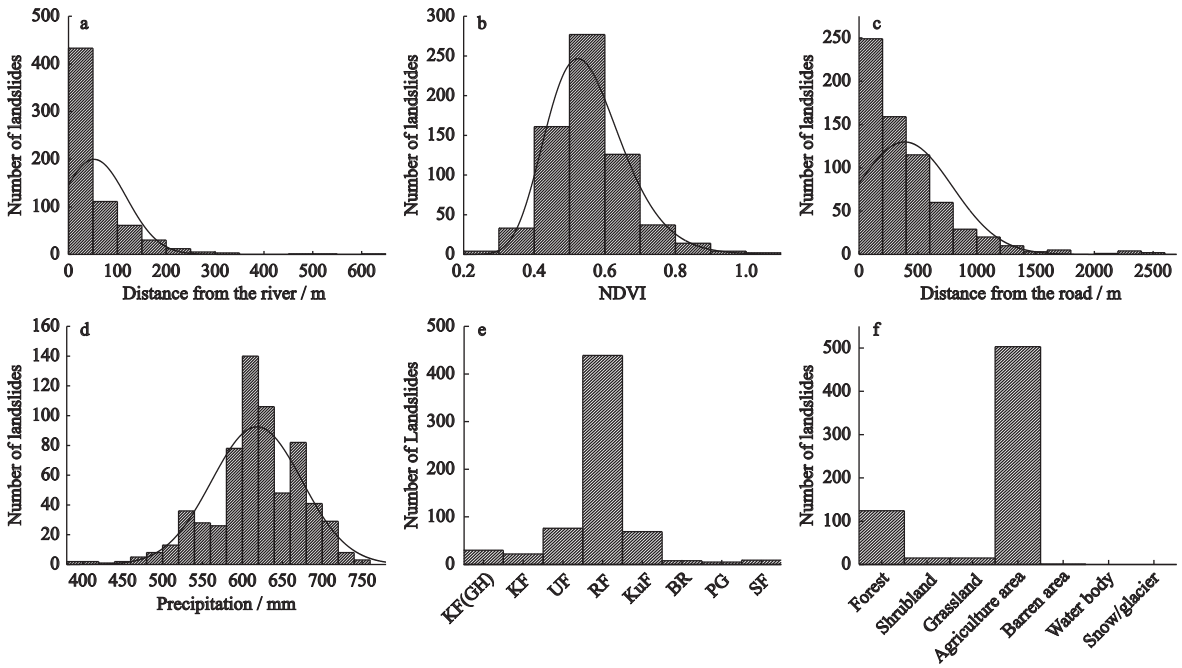

Fig. 6 Distribution of landslides of the Dailekh District in the Western Nepal with different non-topographic factors. a. distance from rivers; b. normalized difference vegetation index (NDVI); c. distance from road; d. precipitation; e. geology; f. land use and land cover (LULC)

formation occupied 11.24% of the total landslide. The land-use and land-cover features clearly influenced the landslide occurrence and distribution. This study showed that more than two-thirds, approximately 76.4%, of the observed landslides existed on agricultural land. It is followed by forest, accounting for 18.8% of all the observed landslides (Fig. 6f). Moreover, small-scale landslides occurred especially in terracing agricultural land, and large-scale landslides occurred on abandoned agriculture terraces, low vegetation coverage areas, and transition places between agricultural land forest or shrub land.

4.3 Landslide susceptibility assessment

For landslide susceptibility assessment, two different models namely, the logistic regression and statistical index methods were applied with the addition of 12 different topographic and non-topographic contributing factors. In the logistic regression, the derived coefficients (β) of each independent variable are shown in Table 1. The coefficients for the logistic regression and the weights for the logistic regression were enrolled to generate the landslide susceptibility mapping coupling with the GIS environment.

For the logistic regression method, a positive coefficient indicates a significant role, whereas a negative coefficient refers to a less significant role of the variable. As shown in Table 1, slope aspect, geology, land use and land cover, TWI, slope, relative relief, and precipitation appeared as the significant factors for landslide susceptibility conditions because of their positive coefficients. The other remaining variables such as altitude, distance from road, distance from rivers, NDVI, and plan curvature showed less contribution on landslide susceptibility.

Then, these 12 different contributing factors and their coefficients were fitted to Eq. (1) to generate a landslide susceptibility map. The logistic regression based susceptibility map was divided into five different hazard classes based on landslide index (LSI) values. These five classes showing LSI value are namely, very low (less than 14%), low (14%–31%), moderate (31%–50%), high (50%–69%), and very high (69%–100%) according to the quantile statistics. As shown in Fig. 7a, 30.4% of regions belongs to very low hazard, with low hazard regions accounting for 21.42%, moderate hazard accounting for 17.33%, and high and very high hazard accounting for 16.69% and 14.15%, respectively.

In the statistical index, the weight of each parameter class was defined as the natural logarithm based on the

Table 1 Independent variables and the corresponding values used in the logistic regression for landslide susceptibility assessment

Parameter	Logistic coefficients
Altitude	−0.551
Aspect	0.022
Distance from the road	−0.395
Distance from the river	−0.770
Geology	0.032
Land-use and land cover	0.565
Normalized difference vegetation index (NDVI)	−0.371
Topographic wetness index (TWI)	0.230
Slope	0.249
Relative relief	0.302
Precipitation	0.025
Plan curvature	−0.623
Constant	1.696

landslide density class divided by the landslide density in the entire map (Table 2). A negative weight values indicates a lower probability of landslide occurrence, whereas a positive weight indicates a higher probability than the average probability of landslide occurrence.

The slope gradients 15°–25°, and 25°–35° have a positive weight of 0.141 and 0.196, respectively. In the case of altitude, classes of < 1000 m and 1000–1500 m represent a positive weight of 0.24 and 0.46, respectively. Regarding aspect, different aspects such as east, southeast, south, southwest, and west have a positive weight; the south aspect has the highest weight of 0.41. The remaining other aspects have negative values showing less probability of landslide occurrence. Regarding the distance from the road, classes of <100 m and 100–500 m have positive values of 0.41 and 0.27, respectively, indicating clear impact of road construction on landslide occurrence. Regarding the distance from river, <100 m distance has clear impact on probability of landslide occurrence, showing a positive value of 0.32. The lesser Himalayan sequences namely, Ranimatta and Kushma formation have positive weights of 0.42 and 0.26, respectively. In the context of land use and land cover, shrubland and agriculture land have the highest positive weight of 0.64 and 0.67. In the case of NDVI, the highest weight was observed in the low vegetation cover class of 0.047−0.543 with value of 0.62, showing a significant role in landslide occurrence. For curvature, weights are positive in convex and concave, which are 0.62 and 0.22; the linear curvature showed a negative value of −0.30. Comparatively, the precipitation classes of 600−650 mm and > 650 mm have positive weights of 0.34 and 0.36 respectively, indicating that heavy rainfall plays a positive impact on landslide occurrence. In the case of relative relief, classes of 200–400 m/km^2 and 400–600 m/km^2 are associated with the positive weights

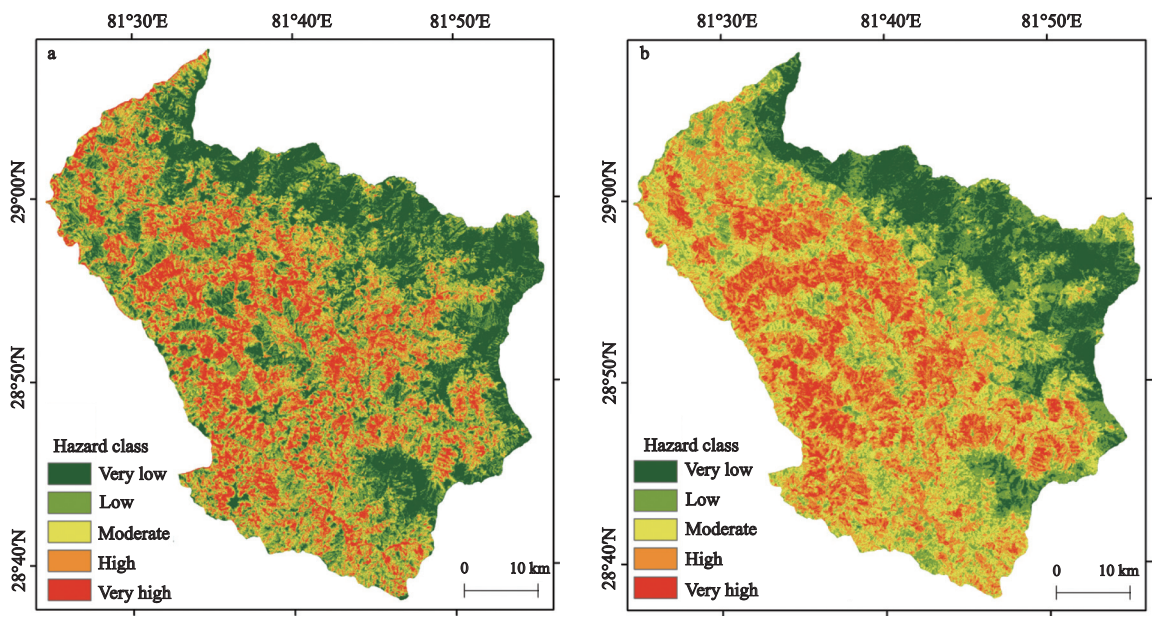

Fig. 7 Landslide susceptibility maps of the Dailekh District in the Western Nepal derived through logistic regression (LR) method (a) and statistical index (SI) method (b)

Table 2 Weights of each class of the triggering factors derived with the natural logarithm in the statistical index method

Variable	Class	W_{ij}	W_{ij} (Ln)	Variable	class	W_{ij}	W_{ij} (Ln)
Altitude / m	< 1000	1.27	0.24	NDVI	< 0.047	0.81	−0.22
	1000−1500	1.59	0.46		0.047−0.543	1.87	0.62
	1500−2000	0.62	−0.47		0.543−0.661	1.25	0.22
	2000−2500	0.05	−2.92		0.661−0.788	0.48	−0.73
	2500−3000	0.00	0.00		> 0.778	0.24	−1.41
	3000−3500	0.00	0.00	Plan curvature	Convex	1.57	0.45
	> 3500	0.00	0.00		Concave	1.16	0.15
Aspect	Flat	0.13	−2.06		Linear	0.74	−0.30
	North	0.45	−0.79	Precipitation / mm	< 400	0.36	−1.02
	Northeast	0.81	−0.21		400−450	0.06	−2.77
	East	1.11	0.11		450−500	0.29	−1.25
	Southeast	1.18	0.16		500−550	0.58	−0.55
	South	1.50	0.41		550−600	0.75	−0.29
	Southwest	1.39	0.33		600−650	1.40	0.34
	West	1.06	0.06		> 650	1.43	0.36
	Northwest	0.66	−0.42	Relative relief /	< 200	0.55	−0.60
Distance from	< 100	1.50	0.41	(m/km^2)	200−400	1.24	0.22
the road /m	100−500	1.31	0.27		400−600	1.13	0.12
	500−1000	0.94	−0.07		600−800	0.48	−0.73
	1000−2000	0.46	−0.78		> 800	0.20	−1.61
	2000−4000	0.17	−1.78	Topographic	1.716−4.460	0.907	−0.10
	4000−6000	0.00	0.00	wetness index	4.460−6.206	1.180	0.17
	> 6000	0.00	0.00		6.206−8.368	1.774	0.57
Distance from	< 100	1.37	0.32		8.368−12.110	0.344	−1.07
the river /m	100−200	0.38	−0.98		12.110−22.920	0.000	0.000
	200−300	0.18	−1.69	Slope / °	< 15	0.590	−0.53
	300−400	0.12	−2.14		15−25	1.151	0.14
	400−500	0.08	−2.54		25−35	1.216	0.20
	500−600	1.05	0.05		35−45	0.850	−0.16
	> 600	0.86	−0.16		> 45	0.328	−1.11
Geology	Proterozoic Himalayan Crystalline	0	0	LULC	Forest	0.30	−1.20
					Shrub land	1.90	0.64
	Kalikot formation (Gh)	0.21	−1.57		Grassland	1.16	0.15
	Kalikot formation	0.28	−1.29		Agriculture area	1.95	0.67
	Ulleri formation	0.74	−0.30		Barren area	0.36	−1.02
	Kalikot formation (Bu)	0.16	−1.85		Water body	0.02	−3.84
	Ranimatta formation	1.52	0.42		Snow/glacier	0.00	0.00
	Kushma Formation	1.30	0.26				
	Basic rocks	0.37	−1.00				
	Palezoic granite	0.25	−1.38				
	Sallyani gad formation	0.30	−1.22				

Notes: W_{ij} is the sum weight of any class *i* of *j* parameter; NDVI, Normalized difference vegetation index; LULC, land use and land cover

of 0.22 and 0.12, respectively. The TWI index classes with a positive weight are the classes of 4.460–6.206 (0.16) and 6.206−8.368 (0.57), whereas negative weights appeared to other classes.

The final landslide susceptibility map was generated using natural logarithm weights of each parameter classes in the statistical index method. Finally, the derived final landslide susceptibility map was divided into

five different classes as the logistic regression method: very low hazard, low hazard, moderate hazard, high hazard, and very high hazard. As shown in Fig. 7b, the landslide hazard classes such as very low, low, moderate, high, and very high landslide susceptibility classes covered 15.73%, 21.25%, 26.65%, 26.03%, and 10.34% of total area. The analysis revealed that the landslide susceptibility is the product of the mutual natural interplay of different topographic and non-topographic triggering factors.

4.4 Comparison and validation

4.4.1 Evaluation with the ROC curve

With the help of the ROC curve, the AUC shows the success rate and prediction rate of both methods. As shown in Fig. 8, among the total 658 of observed landslides, 470 (70%) of all landslides were allocated as the training data, whereas the rest 30% (198 landslides) were selected as the test data. The success rate was calculated with the test data when comparing with the training data, whereas the prediction success rate was derived when comparing the prediction results with the test data. According to the AUC statistics, both the logistic regression and statistical index methods have equal performance, with logistic regression method (success rate, 0.793; prediction rate, 0.826), and statistical index method (success rate, 0.811; prediction rate, 0.823) (Fig. 8). Both methods showed a good and similar prediction rate in landslide susceptibility maps. Hence, these methods can be used for further landslide hazard related activities in the study area.

4.4.2 Evaluation with the R-Index method

The *R*-Index was also applied to evaluate the prediction rate of landslide susceptibility mapping. 658 landslides were utilized to analyze the *R*-Index. As listed in Table 3, the analysis showed that the *R*-Index derived through the logistic regression methods are 1.41, 4.46, 10.47, 26.32, and 57.34 for very low, low, moderate, high, and very high hazard classes, respectively. The statistical index showed the *R*-Index values 0.74, 3.42, 7.30, 22.15, and 66.39 for all hazard susceptibility classes. Comparatively, the statistical index method demonstrated a relatively better prediction accuracy in terms of *R*-Index values than the logistic regression method. However, the highest *R*-Index values were mainly observed to high and very high susceptible classes (Table 3), which also have a good positive correlation with the dense distribution of observed landslides in high and very high susceptible classes.

5 Discussion

5.1 Spatial distribution pattern of landslide

The frequency distribution analysis of the observed landslides concerning different topographic and non-topographic factors showed the degree of relationship between observed landslides and triggering factor classes. Clearly, the majority of landslides are distributed in gentle to moderately steep slopes, consistent with the principle that the evolution of terrains with the cohesion of slope gradients, colluvium rock, and soil materials is strongly related to landslides occurrences

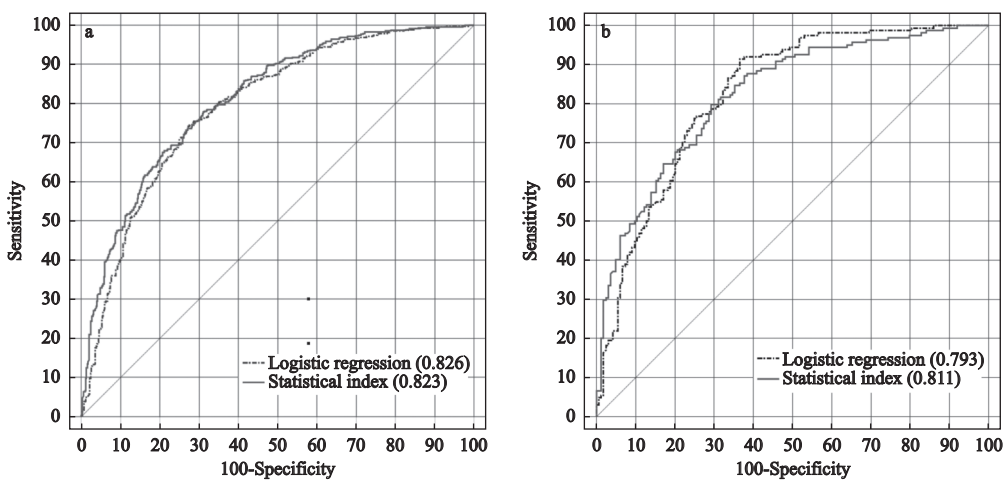

Fig. 8 The receiver operating characteristic (ROC) curve showing the area under the curve (AUC) of the logistic regression method and the statistical index method. a. success rate; b. prediction rate

Table 3 *R*-Indexes showing the accuracy of landslide susceptibility index based on multivariate logistic regression and bivariate statistical index method

Method	Landslide hazard index	Total cell	Area / km^2	Area / %	Total landslide	Landslide / %	*R*-Index
Statistical index method	Very low	583167	233.27	15.73	5	0.76	0.74
	Low	787887	315.16	21.25	31	4.71	3.42
	Moderate	987863	395.15	26.65	83	12.61	7.30
	High	965087	386.04	26.03	246	37.39	22.15
	Very high	383422	153.37	10.34	293	44.53	66.39
Logistic regression method	Very low	1127198	450.88	30.40	18	2.74	1.41
	Low	794042	317.62	21.42	40	6.08	4.46
	Moderate	642545	257.02	17.33	76	11.55	10.47
	High	618855	247.54	16.69	184	27.96	26.32
	Very high	524786	209.91	14.15	340	51.67	57.34

(Selby, 1982; Chorley et al., 1985). A less distribution of landslides in the high steep slopes was influenced by the stability of hard rock, less soil and colluvium materials in the high steep slopes (Chorley et al., 1985). Topographical aspects such as south, east, and west have the most landslides due to characteristics such as retaining of moisture humidity, receiving precipitation, solar radiation, and local wind direction (Selby, 1982; Dai et al., 2001; Zhang et al., 2016; Linkha et al., 2019). A good reciprocal relationship between the coherent condition of relative relief and in situ classes on landslide distribution aligns with the principle that increased local elevation contributes to sufficient potential energy for erosion and mass movement (Ghimire, 2011; Linkha et al., 2019). The curvature types such as convex and concave and their characteristics strongly affect landslide distribution discussed in earlier studies in the Himalaya Mountain region (Mandal and Mandal, 2018). The distribution of two-thirds of observed landslides in the area of lower altitudes is consistent with the mutual interaction of topographic characteristics and human-induced activities such as hillslope-based land-use practices and earthen road construction (Ghimire, 2017; Linkha et al., 2020). The TWI showed a positive relationship with landslide distribution as vertically existing streams have a good saturation showing good signal of landslide occurrence in the study area.

In the case of non-topographic factors, a clear effect of river to landslide occurrence aligns with the principle that geomorphic activities such surface runoff and degree of dissection mainly occur near a close distance to river channels (Selby, 1982; Tucker et al., 2001). The strong effect of vegetation density to landslide occurrence via NDVI has been discussed by previous empirical studies (Xu et al., 2012). Moreover, the results showing a clear influence of the road on the landslide occurrence were supported by some earlier empirical studies (Petley et al., 2007; McAdoo et al., 2018; Linkha et al., 2020). A substantial relationship between the observed landslides and spatial presences of precipitation is consistent with previous empirical studies on precipitation and its role on landslide occurrence in Nepal Himalaya (Dahal and Hasegawa, 2008; Manchado et al., 2021). Different geologic formations such as the Ranimatta, Kusma, and Ulleri formations consisting of phyllites, gneiss (augen) metasandstones, quartzites (white and micaceous), and schists (biotite and feldspathic) rocks have a good coincidence with dense distribution of landslides, as discussed by (Gerrard, 1994). A remarkable association of land-use and land-cover, and its dynamic characteristics resulting in landslide occurrence are consistent with the studies of relationship between landslide and land use and land cover in Nepal (Gardner and Gerrard, 2002). In addition to this, the intensity of long-term land use and land cover change resulted in remarkable environment degradation such as landslides and erosion (Paudel et al., 2016; Ghimire, 2017; Chidi et al., 2021).

The analysis has shown that majority of the landslides have the following characteristics: reoccurrences and repetitive versions of previous patches during precipitation season, resulting in more likely to be enlarged both in form and size, and they have demonstrated a tendency to be deep-seated landslides. These

findings are consistent with previous studies that slope failure events during the monsoon are more responsible for the formation of large-scale landslides in the lesser Himalayas of Nepal (Hasegawa et al., 2009). The new shallow landslides remarkably occurred in the sloppy agricultural land. This triggered the haphazard land-use activities in the steep hillslopes, which was previously concluded in the case of Nepal (Gerrard and Gardner, 2002; Ghimire, 2017). Similarly, the observed landslides and their physical processes have been more proactive during the precipitation season, remarkably contributing to the formation of landslides. Hence, the rainfall-triggered landslides have increased causing tremendous loss of life, fatalities, and property over the succeeding decades in Nepal (Petley et al., 2007).

5.2 Comparison with similar studies in Nepal Himalaya

Landslides are the most common and frequent natural hazards in Nepal Himalaya, causing remarkable loss of lives and damage. Hence, landslide susceptibility mapping is important and a prerequisite activity for landslide hazard-related disaster risk reduction activities in mountainous areas like the Dailekh District. The blind landslide inventory data with 12 different topographic and non-topographic contributing factors were used to generate a landslide susceptibility map of the study area using the logistic regression and statistical index methods. The assessment results show a significant role of the topographic factors including slope, aspect, relative relief, TWI for landslide susceptibility, which have been discussed by previous studies in Nepal Himalaya (Ghimire, 2011; Bijukchhen et al., 2013; Devkota et al., 2013; Dahal, 2014; Dhakal et al., 2020b). In the case of non-topographic factors, geology, land use and land cover, distance from the road, distance from the stream, and precipitation have clearly triggered landslide susceptibility in the study area; this finding is consistent with earlier studies (Hasegawa et al., 2009; Ghimire, 2017; McAdoo et al., 2018; Manchado et al., 2021). The findings are well aligned with the concept that triggering and conditioning factors can vary with the locally existing surrounding situation, leading to dynamic landslide susceptibility mapping results (Dhakal et al., 2020b) because some of the utilized factors appeared as less significant to landslide susceptibility in the study area compared to other previous studies.

The logistic regression and statistical index methods showed a less spatial coverage consisting of dominant observed landslides in the high susceptibility classes. Such a result is consistent with the principle that good susceptibility maps have minimum spatial area and maximum number of landslides (Fell et al., 2008; Dhakal et al., 2020b). The analysis showed a consistent frequency distribution pattern of observed landslides in different susceptibility classes. The AUC values of success rate and prediction rate for logistic regression were 0.793 and 0.826, respectively, which is also consistent with those reported in previous studies (Devkota et al., 2013; Dahal, 2014; Zhang et al., 2019; Amatya, 2020). Likewise, success and prediction rate for the statistical index method is 0.811 and 0.823, respectively, which is also consistent with the findings derived through the previously applied statistical index in Nepal (Bijukchhen et al., 2013; Regmi et al., 2014a). The AUC values of both the methods have a small difference of about 0.003 for the prediction rate. It can be concluded that a mutual interplay of topographic and non-topographic factors including their coherent characteristics contributes to the high landslide hazard susceptibility in the study area. Hence, the derived landslide susceptibility maps using both the methods can be applicable for landslide related hazards and disaster risk management activities.

6 Conclusions

This study focused on analyzing the frequency distribution of landslides and its susceptibility in the Dailekh District, Western Nepal. The logistic regression and statistical index methods were used for landslide susceptibility mapping. In detail, 658 of total blind landslide inventory data and 12 different topographic and non-topographic induced contributing factors were considered for analysis. Among the total of 658 landslides, 460 (about 70%) were allocated for training sample data and the remaining 198 (about 30%) landslides were selected for testing or validation of the final results of landslide susceptibility mapping. The topographic factors included slope, slope aspect, relative relief, curvature, altitude, and TWI while non-topographic factors included distance from the river, NDVI, distance from the road, precipitation, geology, and LULC. The AUC values for success rate and prediction rate of

both the methods were calculated from the ROC curve. The *R*-Index was also applied to evaluate the landslide susceptible prediction capability of both the methods. For both logistic regression and statistical index methods, the ROC-derived prediction AUC values were 0.826 and 0.823, respectively, whereas the success rate values were 0.811 and 0.793, respectively. In the logistic regression, high hazard susceptibility classes have an *R*-Index value of 83.66, whereas in the statistical index approach, high hazard susceptibility classes have an *R*-Index of 88.54. Both methods showed a similar landslide susceptibility in this region. The landslide distribution and susceptibility are the result of a mutually complex natural interplay of various topographic and non-topographic triggering factors.

Overall, this study provided crucial information about landslide activity as well as hazard susceptibility characteristics in the Dailekh District, Western Nepal. Moreover, it confirmed the validity of the two approaches in the Nepal Himalaya region. Both methods played a better and precise role to generate the landslide susceptibility mapping. Therefore, these methods can be useful for landslide related hazard and disaster risk management activities.

References

Adhikari B R, Gautam S, Paudel B, 2022. Landslide, land cover, and land use changes and its impacts in Nepal. In: Sarkar R, Shaw R, Pradhan B (eds). *Impact of Climate Change, Land Use and Land Cover, and Socio-economic Dynamics on Landslides*. Singapore: Springer, 149–164. doi: 10.1007/978-981-16-7314-6_6

Amatya S C, 2020. Challenges of landslide disaster for development in Nepal. *Journal of Development Innovations*, 4(1): 1–19.

Beven K J, Kirkby M J, 1979. A physically based, variable contributing area model of basin hydrology/Un modèle à base physique de zone d'appel variable de l'hydrologie du bassin versant. *Hydrological Sciences Bulletin*, 24(1): 43–69. doi: 10.1080/02626667909491834

Bhandary N P, Dahal R K, Timilsina M et al., 2013. Rainfall event-based landslide susceptibility zonation mapping. *Natural Hazards*, 69(1): 365–388. doi: 10.1007/s11069-013-0715-x

Bijukchhen S M, Kayastha P, Dhital M R, 2013. A comparative evaluation of heuristic and bivariate statistical modelling for landslide susceptibility mappings in Ghurmi-Dhad Khola, east Nepal. *Arabian Journal of Geosciences*, 6(8): 2727–2743. doi: 10.1007/s12517-012-0569-7

Chidi C L, Sulzer W, Xiong D H et al., 2021. Land use intensity dynamics in the Andhikhola watershed, middle hill of Nepal. *Journal of Mountain Science*, 18(6): 1504–1520. doi: 10.1007/s11629-020-6652-8

Chorley R J, Schumm S A, Sugden D E, 1985. *Geomorphology*. Methuen, London and New York: Routledge Kegan & Paul.

Dahal R K, Hasegawa S, 2008. Representative rainfall thresholds for landslides in the Nepal Himalaya. *Geomorphology*, 100(3–4): 429–443. doi: 10.1016/j.geomorph.2008.01.014

Dahal R K, Hasegawa S, Nonomura A et al., 2008. Predictive modelling of rainfall-induced landslide hazard in the Lesser Himalaya of Nepal based on weights-of-evidence. *Geomorphology*, 102(3–4): 496–510. doi: 10.1016/j.geomorph.2008.05.041

Dahal R K, Hasegawa S, Yamanaka M et al., 2009. Comparative analysis of contributing parameters for rainfall-triggered landslides in the Lesser Himalaya of Nepal. *Environmental Geology*, 58(3): 567–586. doi: 10.1007/s00254-008-1531-6

Dahal R K, 2014. Regional-scale landslide activity and landslide susceptibility zonation in the Nepal Himalaya. *Environmental Earth Sciences*, 71(12): 5145–5164. doi: 10.1007/s12665-013-2917-7

Dai F C, Lee C F, Li J et al., 2001. Assessment of landslide susceptibility on the natural terrain of Lantau Island, Hong Kong. *Environmental Geology*, 40(3): 381–391. doi: 10.1007/s002540000163

Devkota K C, Regmi A D, Pourghasemi H R et al., 2013. Landslide susceptibility mapping using certainty factor, index of entropy and logistic regression models in GIS and their comparison at Mugling-Narayanghat road section in Nepal Himalaya. *Natural Hazards*, 65(1): 135–165. doi: 10.1007/s11069-012-0347-6

Dhakal S, Cui P, Rijal C P et al., 2020a. Landslide characteristics and its impact on tourism for two roadside towns along the Kathmandu Kyirong Highway. *Journal of Mountain Science*, 17(8): 1840–1859. doi: 10.1007/s11629-019-5871-3

Dhakal S, Cui P, Su L J et al., 2020b. Landslide susceptibility assessment at Kathmandu Kyirong Highway Corridor in pre-quake, co-seismic and post-quake situations. *Journal of Mountain Science*, 17(11): 2652–2673. doi: 10.1007/s11629-020-6314-x

Dhital M R, Khanal N R, Thapa K B, 1993. *The Role of Etreme Eather Events, Mass Movements, and Land Use Changes in Increasing Natural Hazards: A Report of the Causes of the Recent Damages Incurred in South-central Nepal during 19–20 July 1993*. Kathmandu: ICIMOD.

Dhital M R, 2015. *Geology of the Nepal Himalaya: Regional Perspective of the Classic Collided Orogen*. Switzerland: Springer.

Emberson R, Kirschbaum D, Stanley T, 2021. Global connections between El Nino and landslide impacts. *Nature Communications*, 12(1): 2262. doi: 10.1038/s41467-021-22398-4

Fell R, Corominas J, Bonnard C et al., 2008. Guidelines for landslide susceptibility, hazard and risk zoning for land-use planning. *Engineering Geology*, 102(3–4): 99–111. doi: 10.1016/j.

enggeo.2008.03.014

Froude M J, Petley D N, 2018. Global fatal landslide occurrence from 2004 to 2016. *Natural Hazards and Earth System Sciences*, 18(8): 2161–2181. doi: 10.5194/nhess-18-2161-2018

Gardner R A M, Gerrard A J, 2002. Relationships between runoff and land degradation on non-cultivated land in the Middle Hills of Nepal. *The International Journal of Sustainable Development & World Ecology*, 9(1): 59–73. doi: 10.1080/13504500209470103

Gerrard J, 1994. The landslide hazard in the Himalayas: geological control and human action. In: Morisawa M (ed). *Geomorphology and Natural Hazards*. Amsterdam: Elsevier, 221–230. doi: 10.1016/B978-0-444-82012-9.50019-0

Gerrard J, Gardner R, 2002. Relationships between landsliding and land use in the Likhu Khola drainage basin, Middle Hills, Nepal. *Mountain Research and Development*, 22(1): 48–55. doi: 10.1659/0276-4741(2002)022[0048:RBLALU]2.0.CO;2

Ghimire M, 2011. Landslide occurrence and its relation with terrain factors in the Siwalik Hills, Nepal: case study of susceptibility assessment in three basins. *Natural Hazards*, 56(1): 299–320. doi: 10.1007/s11069-010-9569-7

Ghimire M, 2017. Historical land covers change in the Chure-Tarai Landscape in the last six decades: drivers and environmental consequences. In: Li A N, Deng W, Zhao W (eds). *Land Cover Change and Its Eco-environmental Responses in Nepal*, Singapore: Springer,109–147. doi: 10.1007/978-981-10-2890-8_5

Ghimire M, Timalsina N, 2020. Landslide distribution and processes in the Hills of Central Nepal: geomorphic and statistical approach to susceptibility assessment. *Journal of Geoscience and Environment Protection*, 8(12): 276–302. doi: 10.4236/gep.2020.812017

Guo C W, Huang Y D, Yao L K et al., 2017. Size and spatial distribution of landslides induced by the 2015 Gorkha earthquake in the Bhote Koshi river watershed. *Journal of Mountain Science*, 14(10): 1938–1950. doi: 10.1007/s11629-016-4140-y

Guzzetti F, Carrara A, Cardinali M et al., 1999. Landslide hazard evaluation: a review of current techniques and their application in a multi-scale study, Central Italy. *Geomorphology*, 31(1–4): 181–216. doi: 10.1016/S0169-555X(99)00078-1

Guzzetti F, Reichenbach P, Cardinali M et al., 2005. Probabilistic landslide hazard assessment at the basin scale. *Geomorphology*, 72(1–4): 272–299. doi: 10.1016/j.geomorph.2005.06.002

Hasegawa S, Dahal R K, Yamanaka M et al., 2009. Causes of large-scale landslides in the Lesser Himalaya of central Nepal. *Environmental Geology*, 57(6): 1423–1434. doi: 10.1007/s00254-008-1420-z

Kale V, 2012. On the link between extreme floods and excess monsoon epochs in South Asia. *Climate Dynamics*, 39(5): 1107–1122. doi: 10.1007/s00382-011-1251-6

Kavzoglu T, Kutlug Sahin E, Colkesen I, 2015. An assessment of multivariate and bivariate approaches in landslide susceptibility mapping: a case study of Duzkoy District. *Natural Hazards*, 76(1): 471–496. doi: 10.1007/s11069-014-1506-8

Kopecký M, Čížková Š, 2010. Using topographic wetness index in vegetation ecology: does the algorithm matter? *Applied Vegetation Science*, 13(4): 450–459. doi: 10.1111/j.1654-109X.2010.01083.x

Kubwimana D, Ait Brahim L, Nkurunziza P et al., 2021. Characteristics and distribution of landslides in the populated hillslopes of Bujumbura, Burundi. *Geosciences*, 11(6): 259. doi: 10.3390/geosciences11060259

Lin L, Lin Q G, Wang Y, 2017. Landslide susceptibility mapping on a global scale using the method of logistic regression. *Natural Hazards and Earth System Sciences*, 17(8): 1411–1424. doi: 10.5194/nhess-17-1411-2017

Linkha T R, Rai D K, Lama F, 2019. Landslide hazard mapping: GIS-based susceptibility assessment of Leoutikhola watershed, Dhankuta, Nepal. *The Third Pole: Journal of Geography Education*, 18–19: 71–84. doi: 10.3126/ttp.v18i0.28008

Linkha T R, Rai D K, Khatiwada S P, 2020. Analysis of earthen road construction and land degradation in the Tankhuwakhola watershed of Dhankuta district. *The Geographic Base*, 7: 113–126. doi: 10.3126/tgb.v7i0.34281

Manchado A M T, Allen S, Ballesteros-Cánovas J A et al., 2021. Three decades of landslide activity in western Nepal: new insights into trends and climate drivers. *Landslides*, 18(6): 2001–2015. doi: 10.1007/s10346-021-01632-6

Mandal S, Mandal K, 2018. Bivariate statistical index for landslide susceptibility mapping in the Rorachu River Basin of eastern Sikkim Himalaya, India. *Spatial Information Research*, 26(1): 59–75. doi: 10.1007/s41324-017-0156-9

Martha T R, Roy P, Mazumdar R et al., 2017. Spatial characteristics of landslides triggered by the 2015 M_w 7.8 (Gorkha) and M_w 7.3 (Dolakha) earthquakes in Nepal. *Landslides*, 14(2): 697–704. doi: 10.1007/s10346-016-0763-x

McAdoo B G, Quak M, Gnyawali K R et al., 2018. Roads and landslides in Nepal: how development affects environmental risk. *Natural Hazards and Earth System Sciences*, 18(12): 3203–3210. doi: 10.5194/nhess-18-3203-2018

Meena S R, Ghorbanzadeh O, Blaschke T, 2019. A comparative study of statistics-based landslide susceptibility models: a case study of the region affected by the Gorkha Earthquake in Nepal. *ISPRS International Journal of Geo-Information*, 8(2): 94. doi: 10.3390/ijgi8020094

Paudel B, Zhang Y L, Li S C et al., 2016. Review of studies on land use and land cover change in Nepal. *Journal of Mountain Science*, 13(4): 643–660. doi: 10.1007/s11629-015-3604-9

Petley D N, Hearn G J, Hart A et al., 2007. Trends in landslide occurrence in Nepal. *Natural Hazards*, 43(1): 23–44. doi: 10.1007/s11069-006-9100-3

Poudyal C P, Chang C D, Oh H J et al., 2010. Landslide susceptibility maps comparing frequency ratio and artificial neural networks: a case study from the Nepal Himalaya. *Environmental Earth Sciences*, 61(5): 1049–1064. doi: 10.1007/s12665-009-0426-5

Pradhan A M S, Dawadi A, Kim Y T, 2012. Use of different bivariate statistical landslide susceptibility methods: a case

study of Khulekhani Watershed, Nepal. *Journal of Nepal Geological Society*, 44: 1–12. doi: 10.3126/jngs.v44i0.24483

Regmi A D, Yoshida K, Dhital M R et al., 2013a. Effect of rock weathering, clay mineralogy, and geological structures in the formation of large landslide, a case study from Dumre Besei landslide, Lesser Himalaya Nepal. *Landslides*, 10(1): 1–13. doi: 10.1007/s10346-011-0311-7

Regmi A D, Yoshida K, Nagata H et al., 2013b. The relationship between geology and rock weathering on the rock instability along Mugling-Narayanghat road corridor, Central Nepal Himalaya. *Natural Hazards*, 66(2): 501–532. doi: 10.1007/s11069-012-0497-6

Regmi A D, Devkota K C, Yoshida K et al., 2014a. Application of frequency ratio, statistical index, and weights-of-evidence models and their comparison in landslide susceptibility mapping in Central Nepal Himalaya. *Arabian Journal of Geosciences*, 7(2): 725–742. doi: 10.1007/s12517-012-0807-z

Regmi A D, Yoshida K, Nagata H et al., 2014b. Rock toppling assessment at Mugling-Narayanghat road section: 'a case study from Mauri Khola landslide', Nepal. *Catena*, 114: 67–77. doi: 10.1016/j.catena.2013.10.013

Regmi A D, Yoshida K, Pourghasemi H R et al., 2014c. Landslide susceptibility mapping along Bhalubang—Shiwapur area of mid-Western Nepal using frequency ratio and conditional probability models. *Journal of Mountain Science*, 11(5): 1266–1285. doi: 10.1007/s11629-013-2847-6

Regmi A D, Yoshida K, Cui P et al., 2017. Development of Taprang landslide, West Nepal. *Landslides*, 14(3): 929–946. doi: 10.1007/s10346-016-0752-0

Reichenbach P, Rossi M, Malamud B D et al., 2018. A review of statistically-based landslide susceptibility models. *Earth-Science Reviews*, 180: 60–91. doi: 10.1016/j.earscirev.2018.03.001

Roback K, Clark M K, West A J et al., 2018. The size, distribution, and mobility of landslides caused by the 2015 Mw7.8 Gorkha earthquake, Nepal. *Geomorphology*, 301: 121–138. doi: 10.1016/j.geomorph.2017.01.030

Robinson T R, Rosser N J, Densmore A L et al., 2017. Rapid post-earthquake modelling of coseismic landslide intensity and distribution for emergency response decision support. *Natural Hazards and Earth System Sciences*, 17: 1521–1540. doi: 10.5194/nhess-17-1521-2017

Schmid M O, Baral P, Gruber S et al., 2015. Assessment of permafrost distribution maps in the Hindu Kush Himalayan region using rock glaciers mapped in Google Earth. *The Cryosphere*, 9(6): 2089–2099. doi: 10.5194/tc-9-2089-2015

Selby M J, 1982. *Hillslope Materials and Processes*. Oxford: Oxford University Press.

Shroder J F, Bishop M P, 1998. Mass movement in the Himalaya: new insights and research directions. *Geomorphology*, 26(1–3): 13–35. doi: 10.1016/S0169-555X(98)00049-X

Thapa P B, 2018. Analysis of landslides triggered by the 2015 Gorkha Earthquake, Nepal. In: Kruhl J H, Adhikari R, Dorka U E (eds.). *Living Under the Threat of Earthquakes*. Cham: Springer International Publishing, 45–63. doi: 10.1007/978-3-319-68044-6_3

Tiwari B, Ajmera B, Dhital S, 2017. Characteristics of moderate-to large-scale landslides triggered by the M_w7.8 2015 Gorkha earthquake and its aftershocks. *Landslides*, 14(4): 1297–1318. doi: 10.1007/s10346-016-0789-0

Tucker G E, Catani F, Rinaldo A et al., 2001. Statistical analysis of drainage density from digital terrain data. *Geomorphology*, 36(3–4): 187–202. doi: 10.1016/S0169-555X(00)00056-8

Van Westen C J, 1997. *Statistical Landslide Hazard Analysis ILWIS 2.1 for Windows Application Guide*. Enschede: ITC Publication.

Varnes D J, 1978. Slope movement types and processes. In: Schuster R L, Krizek R J (eds.). *Special Report 176: Landslides: Analysis and Control*. Washington, DC: Transportation Research Board, National Academy of Sciences, 11–33.

Wei K, Ouyang C J, Duan H T et al., 2020. Reflections on the catastrophic 2020 Yangtze river basin flooding in southern China. *The Innovation*, 1(2): 100038. doi: 10.1016/j.xinn.2020.100038

Wilson J P, Gallant J C, 2000. *Terrain Analysis: Principles and Applications*. New York: John Wiley and Sons.

Wubalem A, Meten M, 2020. Landslide susceptibility mapping using information value and logistic regression models in Goncha Siso Eneses area, northwestern Ethiopia. *SN Applied Sciences*, 2(5): 807. doi: 10.1007/s42452-020-2563-0

Xu C, Xu X W, Dai F C et al., 2012. Landslide hazard mapping using GIS and weight of evidence model in Qingshui River watershed of 2008 Wenchuan earthquake struck region. *Journal of Earth Science*, 23(1): 97–120. doi: 10.1007/s12583-012-0236-7

Xue Y G, Kong F M, Li S C et al., 2021. China starts the world's hardest 'Sky-High Road' project: challenges and countermeasures for Sichuan-Tibet railway. *The Innovation*, 2(2): 100105. doi: 10.1016/j.xinn.2021.100105

Yang X K, Huang P, 2021. Restored relationship between ENSO and Indian summer monsoon rainfall around 1999/2000. *The Innovation*, 2(2): 100102. doi: 10.1016/j.xinn.2021.100102

Zhang J Q, Liu R K, Deng W et al., 2016. Characteristics of landslide in Koshi River Basin, Central Himalaya. *Journal of Mountain Science*, 13(10): 1711–1722. doi: 10.1007/s11629-016-4017-0

Zhang J Q, van Westen C J, Tanyas H et al., 2019. How size and trigger matter: analyzing rainfall- and earthquake-triggered landslide inventories and their causal relation in the Koshi River Basin, central Himalaya. *Natural Hazards and Earth System Sciences*, 19(8): 1789–1805. doi: 10.5194/nhess-19-1789-2019